Structural insights into RyR channel gating modulated by intrinsic junctional protein

Hongli Hu (honglihu@cuhk.edu.cn)
Chinese University of Hong Kong, ShenZhen https://orcid.org/0000-0003-3658-272X
Risheng Wei
Peking University
Qiang Chen
The Chinese University of Hong Kong, Shenzhen
Lei Zhang
Peking University
Congcong Liu
Peking University https://orcid.org/0000-0002-8675-9100
Mengxue Zhang
The Chinese University of Hong Kong, Shenzhen
Chuang Liu
Southern University of Science and Technology
Chang-Cheng Yin
Peking University https://orcid.org/0000-0001-7748-3205

Biological Sciences - Article

Keywords:

Posted Date: March 17th, 2022

DOI: https://doi.org/10.21203/rs.3.rs-1434924/v1

Structural insights into RyR channel gating modulated by intrinsic junctional protein

Risheng Wei[1,7], Qiang Chen[2,7], Lei Zhang[3], Congcong Liu[4,5], Mengxue Zhang[2], Chuang Liu[4,6,*], Chang-Cheng Yin[1,*], Hongli Hu[2,*]

[1]Department of Biochemistry and Biophysics, School of Basic Medical Sciences, Peking University, Beijing, 100191, China

[2]Kobilka Institute of Innovative Drug Discovery, School of Life and Health Sciences, The Chinese University of Hong Kong, Shenzhen, Guangdong, 518172, China

[3]Electron Microscopy Analysis Laboratory, Medical and Health Analysis Center, Peking University, Beijing 100191, China

[4]Cryo-electron Microscopy Center, Southern University of Science and Technology, Shenzhen, Guangdong, 518055, China.

[5]Institute for Hepatology, National Clinical Research Center for Infectious Disease, Shenzhen Third People's Hospital, Shenzhen, Guangdong, 518112, China.

[6]Centre for PanorOmic Sciences, LKS Faculty of Medicine, Hong Kong University, Hong Kong.

[7] These authors contributed equally to this work

Correspondence should be addressed to:

Hongli Hu, E-mail: honglihu@cuhk.edu.cn; Chang-Cheng Yin, Email: ccyin@hsc.pku.edu.cn; Chuang Liu, Email: Liuc7@hku.hk;

Abstract

The type-1 ryanodine receptor (RyR1) is an intracellular calcium release channel for skeletal muscle excitation-contraction coupling. Published structures of RyR1 showed RyR1 is open only in the assistance of exogenous regulators, such as caffeine, ryanodine, PCB-95 and diamide. Here, we report that with a mild purification procedure, a single transmembrane protein junctin is co-purified with RyR1. RyR-junctin complex can be activated to open state by Ca^{2+} only. Junctin inserts its transmembrane helix next to S1, S4 and S_{4-5} linker of RyR1, exerting an out-ward pushing force to the TM domain, facilitating the dilation of S6. Junctin regulates the channel conformation by directly affecting the TM domain via Jun/S_{1-4}–S_{4-5} linker. Additional ATP increases the channel open probability by further stabilizing the channel in the open state. Our results demonstrate junctin forms an intrinsic complex with RyR1 and play a key role in the channel gating of RyR1 in physiological context.

Ryanodine receptors (RyRs) are a class of calcium (Ca^{2+}) release channels located in the sarcoplasmic reticulum (SR) membranes of excitable cells, which release Ca^{2+} from SR into cytosol in response to stimuli. RyRs play a key role in Ca^{2+} induced biological process including neural excitation, signal transduction and muscle contraction [1-3]. During excitation-contraction coupling (E-C coupling), the functions of RyRs are modulated by a variety of factors, including proteins (junctin, triadin, calsequestrin(CSQ), calmodulin, FK506-binding protein (FKBP), etc.)[4-8], small molecules (ATP, ryanodine, caffeine, PCB-95, etc.) [9-11]and ions (Ca^{2+}, Mg^{2+}, etc.)[12].

Ca^{2+} and ATP are key endogenous regulators of RyRs. Functional studies demonstrated that Ca^{2+} alone is sufficient to activate RyR channels; the open probability of RyR channel has a bell-shaped Ca^{2+} concentration dependence curve[13-16]. The critical Ca^{2+} activation concentration is 10^{-7} M and the channel open probability increases with the increase of Ca^{2+} concentration at range of 10^{-7}-10^{-4} M[16]. At this concentration range, ATP enhances the open probability of RyR channel. At [Ca^{2+}] 10^{-5}M, ATP increases the channel open probability almost to 100%[17].

Junctin, triadin and CSQ are key proteins located in SR membrane. It is proposed these three proteins in situ might form a quaternary complex with RyR and modulate the channel activity of RyR[8]. Juctin is a 26 kDa single transmebrane (aa23-44) protein[18] located in SR membrane with a short N-terminal part (aa1-22, ~10% of the sequence) facing the cytoplasm and a long C-terminal part (aa45-210, ~80% of the sequence) located in the SR lumen[18,19]. Triadin is a 95 kDa single transmembrane protein with high homology to junctin[19,20]. Both junctin and triadin have KEKE motif in the luminal fragment, which might interact with the positively-charged helix of CSQ, and regulate the RyR channel[7,8,21].

Single channel recording experiments have demonstrated that junctin can enhance the open probability of Ca^{2+}-activated RyR channel. Junctin significantly increase the channel open probability of RyR activated by 10^{-7}M [Ca^{2+}] under the SR lumen [Ca^{2+}] ~10^{-3}M [20,22].

The RyR structures have been studied exhaustively by cryo-electron microscopy, with structures of open and closed states captured[23-34]. All of the current open-state structures were obtained in the assistance of exogenous pharmacological activators, such as caffeine, ryanodine, PCB-95 and diamide[25,28,31,34-36]. Contradictory to functional studies, the RyR channel can be activated only to a 'primed' state by Ca^{2+} alone or even in the presence of ATP[25,31], in which, the gate is not fully open for Ca^{2+} release. The contradiction between structural studies and functional studies still remains a mystery. The structural studies are based on purified RyR

samples whereas some functional studies based on partially purified RyR samples or even SR vesicles, which suggests that some key factors might be missing in the purified RyR samples, leading to the loss of RyR1 full activation by Ca^{2+} and Ca^{2+}/ATP in the structural studies.

Here, we report that by a mild purification procedure, we obtained an RyR1-junctin complex. Structural studies of this RyR1-junctin complex revealed that RyR1-junctin complex can be activated by Ca^{2+} or Ca^{2+}/ATP to open state. In the Ca^{2+} alone sample, two Ca^{2+} activated structures were obtained, corresponding to primed and open states respectively. In the Ca^{2+}/ATP sample, only one structure was obtained corresponding to full open state. Detailed structural analysis revealed that junctin interacts with RyR1 by inserting its transmembrane helix into the RyR1 transmembrane domain at position next to S1, S4 and S_{4-5} linker by hydrophobic interactions. These interactions exert an out-ward pushing force to the RyR1 transmembrane domain. This pushing force acts synergically with Ca^{2+} or Ca^{2+}/ATP, which exert a pull force to the RyR1 S6 from the top, greatly facilitate the dilation of S6, thus the opening of RyR1 channel. Our work demonstrates junctin forms an intrinsic complex with RyR1 and play a key role in the channel gating of RyR1 in physiological context.

Results

Junctin forms an intrinsic complex with RyR1

When we purified the RyR1 by sucrose gradient sedimentation[37,38], we discovered a protein with an apparent molecular mass between 25-35 kDa co-migrated with RyR1 (Fig. S1a). According to this apparent molecular mass, we infered this protein as junctin. To identify this protein, we performed mass spectroscopy analysis on this protein, and compared the peptide finger prints with data base. As shown in Fig.S1b and S1c, six finger print peptides (boxes 1-6 in Fig.S1b) from mass spectroscopy match with the sequence of rabbit cardiac junctin and they cover different sequence fragments across junctin (Fig.S1d), but these sequence fragments are different from other species (e.g. human, canine, and mouse cardiac muscle) in junctin. The peptide finger prints identify this protein as junctin. The co-migration of junctin with RyR1 in sucrose gradient sedimentation suggests that junctin forms a complex with RyR1. As this complex is directly purified from SR membranes, this suggests junctin is an intrinsic part of the RyR1 complex (we denoted the sample containing junctin as native RyR1). To confirm junctin as an intrinsic part of RyR1 complex, we then performed cryo-electron microscopy studies on the RyR1 sample containing junctin.

In the samples with junctin, an extra helix together with a loop appear in the RyR1 transmembrane domain, whereas in the samples without junctin, the extra helix and loop are

missing. The structural data indicate this extra helix with a loop is contributed by junctin. The predicted model of transmembrane helix together with the loop of junctin (sequence SFFTWFMVI ALLGVWTSVA VVWFDL) matches well with the EM density map (Fig.S1c). The junctional protein triadin was not detected in SDS-PAGE gel and mass spectroscopy (Fig.S1a). Several other proteins exist in the RyR1 samples containing junctin, which are identified as Ca^{2+}-ATPase, junctophilin and CSQ by mass spectroscopy. Ca^{2+}-ATPase and CSQ are ruled out as the single transmembrane helix contributors since Ca^{2+}-ATPase is a protein with 10 transmembrane helices whereas CSQ is a soluble protein with no transmembrane helix[39]. Junctophilin is also ruled out as the predicted transmembrane helix of junctophilin (sequence NS VMIVLVMLLN IGLAILFVHFL) does not match the EM density map.

To elucidate how junctin interacts with RyR1, we performed detailed structural analysis of junctin with RyR1 (Fig. 1). Structural analysis reveals that the transmembrane helix of junctin is located in the RyR1 transmembrane domain, adjacent to S1 and runs parallel with S1; the loop is located in the SR luminal side and runs roughly parallel with the membrane plane (Fig. 1a, 1b). The interactions between junctin and RyR1 are mainly hydrophobic: on the cytoplasmic side, a cluster of hydrophobic residues of junctin (F23, F24, W26, F27) interact with S1 (L4567, F4571, F4568), S4 (V4820, I4816, A4817, L4813) and $S_{4\text{-}5}$ linker (L4823) of RyR1 (Fig. 1c ,1e, S5b, S5c); on the luminal side, hydrophobic residues of junctin (I30, L33, W36) interact with F4575, F4579 of S1 of RyR1 (Fig. 1d ,1f, S5b, S5c). We infer through these interactions, junctin may provide a pushing force to RyR1 transmembrane domain and facilitate the gating of RyR1 as a channel regulator.

Junctin facilitate the gating of RyR1 channel by Ca^{2+} and ATP

To study whether junctin affects channel gating by Ca^{2+} and ATP, we performed cryo-EM of RyR1-junctin complex in the presence of Ca^{2+} and Ca^{2+}/ATP, and compared with the RyR1 structures without junctin. We performed cryo-EM at 5 different conditions: (1) purified RyR1 in the absence of junctin and Ca^{2+} (5 mM EGTA, denoted RyR1-EGTA); (2) purified RyR1 in the presence of Ca^{2+} alone (RyR1 + 100 nM Ca^{2+}, denoted RyR1-nM[Ca^{2+}]); (3) native RyR1-junctin in the presence of Ca^{2+} alone (RyR1-junctin + 100 nM Ca^{2+}, denoted RyR1-Jun/nM[Ca^{2+}]; (4) purified RyR1 in the presence of Ca^{2+} and ATP (20 μM Ca^{2+} + 2 mM ATP, denoted RyR1-μM[Ca^{2+}]/ATP); (5) native RyR1-junctin in the presence of Ca^{2+} and ATP (RyR1-junctin + 20 μM Ca^{2+} + 2mM ATP, denoted RyR1-Jun/μM[Ca^{2+}]/ATP). Condition 1 was used to obtain the RyR1 structure at resting (closed) state; condition 2 was used to obtain the purified RyR1 structure at critical Ca^{2+} activation concentration; condition 3 was used to

see the effect of junctin on the gating of RyR1 by Ca^{2+} alone at critical Ca^{2+} activation concentration; condition 4 was used to obtain the purified RyR1 structure activated by Ca^{2+} and ATP; and condition 5 was used to see the effect of junctin on the gating of RyR1 by Ca^{2+} and ATP. The data collection and image processing procedures are outlined in Fig. S2 and the data collection and model statistics are summarized in Table S1. Altogether, six different structures were obtained (Fig. S3). These structures can be classified into four categories according to the activation states, namely closed, pre-open (primed), activated shut, activated open and full open states (Fig.S6, a-f).

The mushroom-like cytoplasmic region of RyR has "breathing" motion when the channel is transiting from closed state to open state, obvious expansion of outside shell and downward rotation of core region are observed. As shown in Fig2b， upon the Ca^{2+} loading(RyR1-100nM[Ca^{2+}]), the shell region, including NTD, Helical domain (HD1), and Handle domain, move outward from the central axis and downward toward SR membrane, while the central domain contracts, thus the whole cytoplasmic structure is expanded[40]. CTD, VSD and TM domain remain inactive, leading the structure to the pre-open state (Fig. 2b). In the presence of junctin (RyR1-Jun/nM[Ca^{2+}]), we observed additional outward movement of handle domain, central domain and TM domain (S1, S4 and S6) (Fig.2c). The pore diameter increases from 6.2Å to 13.8Å, thus inducing the channel to open state for Ca^{2+} release (Fig.S6e, S6j, S6m). The distance of diagonal I4937 in the gate is even larger than RyR-Ca^{2+}/ATP/caffeine that was reported by des Georges [25] and RyR1 activated by Ca^{2+}/ATP/caffeine/CHL from Ruifang Ma[28]. Interestingly, when analysing the data of RyR1-Jun/nM[Ca^{2+}], we also obtained one 3D structure whose gate remains inactivated, while the conformation is different from the previously reported pre-open state, namely activated shut state (Fig.S2, S3c, S6d, S6i). The shut state was obtained from 60% of the particles (Fig.S7). The shut state has a relative larger gate size (6.8Å) (Fig.S6d) than the pre-open state (6.2Å) (Fig.S6b) in TM region, however, the cytoplasmic domain has a larger expansion than pre-open state (Fig.S8a). The existence of shut and open state in RyR1-Jun/nM[Ca^{2+}] sample shows that junctin together with nM [Ca^{2+}] can activate the RyR in open state to allow hydrated Ca^{2+} to release, and the open probability is only 40%.

Since both Ca^{2+} and ATP are important activators of RyR1, we further compared the structures of RyR1 with/without junctin in presence of 20μM Ca^{2+} and 2mM ATP. In condition 4 (RyR1-μM[Ca^{2+}]/ATP), μM[Ca^{2+}]/ATP can induce a large conformational change of cytoplasmic domain, but not sufficient for S6 dilation. ATP interacts with CTD and U-motif,

to further stabilize the calcium activated central domain. The TM helix remains the same size as in nM [Ca^{2+}] (Fig.2d, S6c, S6k, S6m). For the sample of RyR1-Jun/μM[Ca^{2+}]/ATP, the RyR1 is in an open conformation with a large outward shift of CTD, U-motif and TM helix. The pore diameter is 15.1Å (Fig.2e and Fig.S6f, S6l, S6m), which is more expanded than the previous observed open state. We name this conformation as full open state. In this sample, only the full open structure is observed, thus the open probability is 100%.

Junctin induced the conformational transitions of RyR1 in cooperation with Ca^{2+}/ATP

To understand the synergic regulations of the junctin, Ca^{2+} and ATP, we compared the conformational transitions of RyR in closed state (RyR1-EGTA) and activated open state (RyR1-Jun/nM[Ca^{2+}]). The global transition contains complicated domains cooperation in the core region, e.g. central domain, VSC, CTD and TM domain (Fig.3a). The interface among these four domains is called O-ring[36]. The high-affinity Ca^{2+} binding site locates at the interface between α10, α13, α16 at central domain and H3-H4 loop at CTD, which brings central domain and CTD in a closer adjacent (Fig.S4k, S4m-n). The movement of central domain causes in-ward shift of α4 and an out-ward shift of α22 and α21 (i.e, U-motif). The interaction between α4 and C3'/C2, the interaction between α22 and S2' of VSC domain, enable an outward movement of VSC domain (Fig.3 b-c, S5 e-f). The changes of S2' and S3' of VSC are transmitted to S2 and S3 in TM domain, exerting a pushing force to TM S_{1-4}. Since the signal transduction is through a long-range allosteric gating from central domain to the TM domain[25,32], we name it as α4/Umotif-VSC-S_{1-4}–S_{4-5} linker-gate path. In the other hand, CTD is also clamped by the U-motif via a hydrophobic chamber and transfers the movement directly to S6 of TM domain. Since the four residues I4937 of S6 from RyR tetramers form the gate of Ca^{2+} release, the movement of CTD directly pull the trigger for channel opening. This signal transduction is named as Umotif/CTD-S6 path. The endogenous regulator junctin inserts into the membrane adjacent to S1 and S4, which cause a large outward shift of S1 and S2 (Fig.2c, 3e, 3f). Besides, the cytoplasmic side of junctin has hydrophobic interaction with S_{4-5} linker, which pulls S_{4-5} linker away from the central axis. The hydrophobic interaction between S_{4-5} linker (I4826, V4830, H4832, N4833) and S6 (F4940, E4942, A4939, I4936) can facilitate the dilation of S6 (Fig.S5g) [25].

In the previous reported RyR1 open structures, RyR1 can only be fully activated with the assistance of exogenous regulators, such as ATP/Caffeine, ryanodine, PCB-95 and diamide[25,28,31,34,36]. ATP interacts with H2 of CTD, α21 of U-motif and cytoplasmic side of S6 (Fig.2d, S4l, S4o). Caffeine interacts with α4, VSC, CTD and α22, locking the central domain

in a contracted state. The additional ATP/Caffeine enhances the signal transmission of both α4/Umotif-VSC-S_{1-4}–S_{4-5} linker-gate path and Umotif/CTD-S6 path, leading to S6 dilation. PCB95 can also strength the contraction of central domain[26]. The diamide insecticide (CHL) interacts with TM S_{1-4}, inducing a displacement of S_{4-5} linker, causing movement of S5 and S6 to open the pore[28]. In our activated open structure (RyR1-Jun/nM[Ca^{2+}]), in presence of low concentration Ca^{2+}(nM), junctin by itself can exert a pushing force to the TM domain, which is sufficient to open the channel. RyR can be fully activated by the cooperation of endogenous regulators junctin and Ca^{2+}, with the open probability of 40% (Fig.S7).

Although in the physiological membrane, RyR can be fully activated by μM[Ca^{2+}]/ATP, our structure (condition 4, RyR1-μM[Ca^{2+}]/ATP) shows that purified RyR1 is in pre-open state in presence of μM[Ca^{2+}]/ATP. However, there is only one structure in full open state with the native RyR/junctin complex (RyR-Jun/μM[Ca^{2+}]/ATP). The overall structures of the upper part of O-ring at pre-open and full-open state are very similar, α4, α10, α13, α16, α19(central domain) and H3-H4 loop (CTD) are barely moved. The regions that interacting with TM domain have small out-ward movement, such as U-motif (α20′, α21, α22), CTD (H2, H3) and VSC (S2′, C2, C3) (Fig.3g-3i). As expectation, the TM domain S1, S2 and S_{4-5} linker are pushed outward by the insertion of junctin (Fig.3j, 3k). We noticed that the Ca^{2+} and ATP binding sites are similar to the pre-open state except the global movement of these sub-regions, which may indicate the initiation of conformational changes is from TM regions. In the activated open and full open structures, I4937 in RyR1 channel can both be open for Ca^{2+} release with the help of low concentration of Ca^{2+}. We speculated that junctin is the key trigger here to directly pull S6 outward through TM S_{1-4}. We name it as Jun/S_{1-4}–S_{4-5} linker-gate path, which is independent from the conformation of cytoplasmic domains. Additional mM concentration of ATP can increase the open probability by locking the interface between CTD and S6.

RyR1 activation is regulated by different allosteric communication pathway

The modulation of RyR1 is crucial for channel activities and calcium homeostasis in cell. While multiple type modulators, such as proteins, small molecules and ions can synergistically regulate the channel kinetics in situ[7,9,22]. The channel open probability primarily depends on calcium concentration in cytoplasm with a bell-shaped curve. RyR1 is in closed state when the Ca^{2+} concentration is lower than nano-molar, e.g. RyR-EGTA(Fig.4a). When activated by Ca^{2+} at concentration between nano-molar and micro-molar level, Ca^{2+} binds to the high-affinity binding site at the central domain, leading to the conformational changes of the neighboring

structures, e. g. α4, CTD and U-motif, then the channel is activated in pre-open state but the gate remains closed (Fig.4b). However, Ca^{2+} alone, even with the help of mM concentration ATP, is not sufficient to drive the channel to the open state (Fig.4e). ATP interacts with the CTD, U-motif and cytoplasmic S6 and regulates the channel open probability by pulling S6 outward directly. While in our structure (condition 4), the gate has the same size as pre-open state (Fig.S6b-c). Additional caffeine can lock the α4 in central domain to a more contracted conformation, thus to enhance the pulling force from ATP to S6 (Fig.4f) [31]. ATP/Caffeine can active the RyR1 channel through α4/Umotif-VSC-S_{1-4}–S_{4-5} linker-gate path and Umotif/CTD-S6 path (Fig.4g). Besides, 37% of the particles of RyR1 in Ca^{2+}/ATP/Caffeine were activated, the rest have a closed gate, which is corresponding to the shut state we reported here (Fig.S7) [31].

In our study, RyR1 can be activated by a mechanism without help of ATP/Caf. Junctin inserts into the SR membrane, in adjacent to the RyR S1-S4 helix, pushing the TM helix outward from the central axis. Besides, junctin also interacts with S_{4-5} linker, exerting a pulling force to S6 to facilitate the pore open. Junctin regulates the channel conformation by directly affecting the TM domain via Jun/S_{1-4}–S_{4-5} linker-gate path (Fig.4g), which is similar to the mechanism modulated by insecticide CHL. Jun/S_{1-4}–S_{4-5} linker-gate path facilitate S6 dilation from bottom to up which promote 40% channel to open state. Additional ATP increases the P_0 and further stabilizes the channel in open state (Fig.4c, 4d).

Discussion

Junctin is critical for channel open in native environment

Single channel recording experiments showed that in its native membrane environment, RyR1 can be activated by Ca^{2+}/ATP, in 10^{-7}-10^{-5}M Ca^{2+} range. The open probability increases with Ca^{2+} concentration, and it increases to P_0~1 with additional mM concentration ATP[17]. However, the purified RyR1 are in pre-open state with a closed pore under the buffer condition of μM Ca^{2+} and mM ATP, as described in our sample RyR1-μM[Ca^{2+}]/ATP as well as previous reported structures in 50 μM Ca^{2+} and 7mM ATP[35]. Since the structures were solved with purified RyR1, the open probability may not stay the same as in the native membrane. In our samples of RyR1 with junctional protein junctin, we obtained the structures which are consistent with single channel recording experiments. RyR1-Jun complex can be activated by a low Ca^{2+} concentration (nM), however, at the same time, 60% proteins are still in shut state. With μM[Ca^{2+}]/ATP, all the channels are in full open state, corresponding to the open

probability as 100%. The channel open probability depends on the calcium concentration and ATP in its environment, as shown in single channel recording experiments. These results indicate that without the exogenous regulator, such as Caffeine, PCB95 and CHL, the endogenous regulator junctin plays a critical role to facilitate the pore open in the native SR membrane.

Junctin promote RyR1 into shut state at nM Ca^{2+} that is distinguished from pre-open state

According to the bell-shaped Ca^{2+} action curve, RyR1 activation probability P_0 increases at nM Ca^{2+} concentration and is highest at μM Ca^{2+}. With the association regulator junctin, majority (60%) of RyR1 is facilitated to shut state at low concentration (nM) Ca^{2+}. Although the pore remains closed, the shut state presents a more expansion on cytoplasmic domains than the pre-open state, indicating an intermediate conformation between pre-open and open state (Fig.S8). To investigate the domains transitions upon RyR1 activation, we compared the conformational changes from pre-open to shut state, then to the open state. The core regions, e.g. α4, U-motif, VSC and CTD in shut state is similar to pre-open, but outer shell (NTD, HD1 and Handle domain) is more expanded from the central axis (Fig.S8a, S8b). Besides, junctin interacts with the TM domain, so the TM S_{1-4} and its adjacent VSC domain also move outward but without pore dilation. When RyR1 is further activated to the open state, the fundamental changes are shift at TM S_{1-4} and S6 to allow channel open. All of the domains located in outer shell and core regions (NTD, HD1, handle domain, α4, U-motif, VSC and CTD) moved outward to adapt the pore dilation (Fig.S8c-S8h). Among these domains, since VSC interacts with TM domain and central domain, the conformational changes at TM domain would cause an obvious movement of VSC, and we observed that S2', C2, C3 and S3' have a larger shift when RyR changes from shut to open state. In addition, CTD also have a larger movement from shut to open. This sub-region in O-ring is not stabilized with Jun/Ca^{2+} only sample, so only 40% receptors are in open state and 60% receptors are still in shut state. Since α22 from U-motif interacts with S2' of VSC domain and CTD is also clamped by the U-motif, additional ATP in the sample interacts with H2 of CTD, α21 of U-motif, which help to lock the structure of CTD and VSC in the full open state.

Methods

RyR1purification

RyR1 was purified from CHAPS-solubilized skeletal heavy SR essentially as described previously with modifications[37,38]. Briefly, skeletal heavy SR vesicles were suspended in buffer A (0.2 M NaCl, 20 mM Na-HEPES, pH 7.4, 2 mM DTT, 2 mM PMSF, 1:1 000 diluted protease inhibitor cocktail (Sigma-Aldrich, P8340) and 1.2% CHAPS (AMRESCO)/0.6% soybean lecithin (Sigma-Aldrich, 11145); the CHAPS/protein ratio was 12:1 (wt/wt)). The sample was centrifuged for 1 h at 110 000× g after incubation on ice for 30 min with shaking. The supernatant was loaded onto a 5-ml hydroxyapatite ceramic (Bio-Rad) column equilibrated with buffer B (200 mM NaCl, 10 mM Na-HEPES, pH 7.4, 0.5% CHAPS/0.25% soybean lecithin, 2 mM DTT, 2 mM PMSF, 1:1 000 diluted protease inhibitors cocktail). The column was washed with buffer B containing 10 mM K_2HPO_4, followed washing with buffer B containing 50 mM K_2HPO_4. Proteins were then eluted with 15 ml of buffer B containing 200 mM K_2HPO_4. The eluate was collected and concentrated by centrifugation at 1 000× g in a 100-kDa cut-off Amicon centrifugal filter (Millipore) and stored in small aliquots at −80 °C. The purified RyR1 samples are prepared by loading the sample onto the top of a 5% - 20% (w/v) linear sucrose gradient in buffer B. After centrifugation for 16 h in a Beckman SW28 rotor at 26 000 rpm, the gradient was fractionated into 1.5-ml fractions. The fractions containing RyR1 were collected for the cryo-EM analysis. The mild purified samples were prepared by omitting hydroxyapatite ceramic affinity chromatography column. The fractions containing RyR1 and junctin were collected for cryo-EM analysis.

Mass Spectroscopy

The mild purified RyR1 sample was loaded to a home-made 4%-12% SDS-PAGE gel and run for 90 min at 120V. The gel was detected by silver staining and washed with milli-Q water to remove the background stain. To identify the proteins that co-migrate with RyR1, the gel slice for mass spectroscopy analysis was cut out before the protein bands were separated to identify proteins in the sample. The gel slice corresponding to molecular weight of 26 kDa (green box in Fig.S1a) was cut from the gel and further diced in $1mm^3$ cubes and then hydrolyzed with trypsin. In LC-MS/MS analysis, digested products were separated by a 120 min gradient elution at a flow rate 0.300 µL/min with the Thermo Ultimate 3000 nano-UPLC system which was directly interfaced with the Thermo Fusion LUMOS mass spectrometer. The analytical column was an Acclaim PepMap RSLC column (75 µm ID, 250 mm length, C18). Mobile phase A consisted of 0.1% formic acid, and mobile phase B consisted of 100% acetonitrile and 0.1% formic acid. The Fusion LUMOS mass spectrometer was operated in the data-dependent acquisition mode using Xcalibur 4.1.50 software and there is a single full-scan mass spectrum in the Orbitrap (375-1500 m/z, 60,000 resolution) followed by data-dependent MS/MS scans. The MS/MS spectra from each LC-MS/MS run were searched against the selected database using the software Proteome Discovery (version 2.2)

RyR1 sample preparation for cryo-EM and data collection

The purified and native RyR1 samples are incubated with the corresponding buffers (EGTA, Ca^{2+}, ATP) conditions 1-5 for one hour before plunge freeze. Aliquots of 3µl of RyR1 at a

concentration of approximately 25nM is applied to glow-discharged Lacey carbon grids (400-mesh CuTED PELLA). Grids were transferred to FEI Titan Krios electron microscope (Thermo-Fisher) that was operating at 300 kV. Images were collected automatically using software EPU and recorded in movie mode using FEI Falcon-III detector at a nominal magnification of 75,000×, corresponding to a pixel size of 1.09 Å. A dose fractioned data collection was used to take each micrograph with 30 frames, resulting a total dose of 50 e^- per $Å^2$. A total number of 2265/5364/6454/7665/6633 movie stacks for RyR1 samples in conditions 1-5 were obtained with the defocus range 1.2-2.2 μm.

Cryo-EM data analysis

For all of the datasets, the movie frames were further processed with MotionCorr2 for the motion correction and dose weighting[41]. The contrast transfer function parameters were estimated by Gctf[42]. Similar image processing procedures were performed on all the dataset and the details are shown in Fig.S2. With regard to the dataset of condition 1(RyR1-EGTA), 2265 micrographs were obtained after evaluation with CTF parameters. 443,814 particles were picked automatically with Laplacian-of-Gaussian approach and extracted in Relion 3.0/3.1 [43]with a binned pixel size of 2.18Å. After 2 rounds of 2D classification and 2 rounds of 3D classification, the particles were cleaned up and re-centered, re-extracted with the original pixel size of 1.09Å. The remaining 60,110 good particles were imported into CryoSPARC v3.2.0[44], and subjected into a non-uniform refinement, which yield a reconstruction at 4.0 Å (C4 symmetry). The resolution estimation was reported according to the gold-standard Fourier shell correlation (FSC) using the 0.143 criterion. The local resolution map was calculated by Blocres[45]. For the datasets of condition 2 (RyR1-100nMCa^{2+}), condition 4 (RyR1-μMCa^{2+}/ATP) and condition 5 (RyR1-Jun/μMCa^{2+}/ATP), the individual particles stacks with the number of 183,859/114,423/103,688 were reconstructed into 3.4Å, 3.9Å and 3.9Å, respectively.

For the dataset of condition 3(RyR1-Jun/nMCa^{2+}), an ab inito reconstruction and one round of heterogeneous refinement were performed after imported into CryoSPARC and resulted in two different classes. After the non-uniform refinement, one class of 78,641 good particles yield a reconstruction of RyR1 in shut state at 3.8 Å and another class of 52,414 particles with a reconstruction of RyR1 in open state at 4.2Å.

Model building, refinement, analysis

To build the structural models, a recently published structure (PDB ID: 6WOT) was used as the initial model[27]. This structure was modified and docked into the density maps by CHIMERA[46]. The atomic models were then refined against maps iteratively by cycles of real space refinement in PHENIX with secondary structure and geometry restrained[47]. The refined models were further manually improved in Coot[48]. Extensive reports on evaluation were provided by the PHENIX comprehensive validation program. The analysis of pore dimensions was conducted using HOLE and illustrated in VMD[49].

Acknowledgement

We thank State Key Laboratory of Natural and Biomimetic Drugs, Peking University for the

mass spectroscopy analysis of junctin component. We thank Cryo-EM Centre and Department of Biology, Southern University of Science and Technology, Shenzhen for Cryo-EM data collection.

This work was supported by the National Key Research and Development Program of China (Grant No. 2017YFA0504700) and the National Natural Science Foundation of China (Grant No. 31770785) to C.C.Y. This work was in part supported by the National Natural Science Foundation of China, Youth Science Fund (Project No. 31900868, to C.L and 32100963, to H.H), Shenzhen Science and Technology Innovation Committee (Projects No. JCYJ20210324131802008, to H.H). This work was also supported by Kobilka Institute of Innovative Drug Discovery and Presidential Fellowship and University Development Fund at the Chinese University of Hong Kong, Shenzhen (H.H, Q.C).

Author contributions

R.W performed the protein purification and mass spectroscopy analysis; C.L, C.C.L and Q.C performed the EM analysis, collected the cryo-EM data, performed image processing and 3D reconstruction; R.W and C.Y analyzed the data; C.L, C.Y and H.H initiated the project, supervised the research, and wrote the manuscript.

Competing interests

The authors declared no competing interests.

References

1 Pessah, I. N., Waterhouse, A. L. & Casida, J. E. The calcium-ryanodine receptor complex of skeletal and cardiac muscle. *Biochem Biophys Res Commun* **128**, 449-456, doi:10.1016/0006-291x(85)91699-7 (1985).

2 Agnew, W. S. Excitation Contraction Coupling - Proteins That Bridge the Gap. *Nature* **334**, 299-300, doi:DOI 10.1038/334299a0 (1988).

3 Lanner, J. T., Georgiou, D. K., Joshi, A. D. & Hamilton, S. L. Ryanodine receptors: structure, expression, molecular details, and function in calcium release. *Cold Spring Harb Perspect Biol* **2**, a003996, doi:10.1101/cshperspect.a003996 (2010).

4 Tripathy, A., Xu, L., Mann, G. & Meissner, G. Calmodulin activation and inhibition of skeletal muscle Ca2+ release channel (ryanodine receptor). *Biophys J* **69**, 106-119, doi:10.1016/S0006-3495(95)79880-0 (1995).

5 Jeyakumar, L. H. *et al.* FKBP binding characteristics of cardiac microsomes from diverse vertebrates. *Biochem Biophys Res Commun* **281**, 979-986, doi:10.1006/bbrc.2001.4444 (2001).

6 Beard, N. A. & Dulhunty, A. F. C-terminal residues of skeletal muscle calsequestrin are essential for calcium binding and for skeletal ryanodine receptor inhibition. *Skelet Muscle* **5**, 6, doi:10.1186/s13395-015-0029-7 (2015).

7 Zhang, L., Kelley, J., Schmeisser, G., Kobayashi, Y. M. & Jones, L. R. Complex formation between junctin, triadin, calsequestrin, and the ryanodine receptor. Proteins of the cardiac junctional sarcoplasmic reticulum membrane. *J Biol Chem* **272**, 23389-23397, doi:10.1074/jbc.272.37.23389 (1997).

8 Gyorke, I., Hester, N., Jones, L. R. & Gyorke, S. The role of calsequestrin, triadin, and junctin in conferring cardiac ryanodine receptor responsiveness to luminal calcium. *Biophys J* **86**, 2121-2128, doi:10.1016/S0006-3495(04)74271-X (2004).

9 Kong, H. *et al.* Caffeine induces Ca2+ release by reducing the threshold for luminal Ca2+ activation of the ryanodine receptor. *Biochem J* **414**, 441-452, doi:10.1042/BJ20080489 (2008).

10 Gong, D. S., Yan, N. E. & Ledford, H. A. Structural Basis for the Modulation of Ryanodine Receptors.

Trends Biochem Sci **46**, 489-501, doi:10.1016/j.tibs.2020.11.009 (2021).
11 Xu, L., Mann, G. & Meissner, G. Regulation of cardiac Ca2+ release channel (ryanodine receptor) by Ca2+, H+, Mg2+, and adenine nucleotides under normal and simulated ischemic conditions. *Circ Res* **79**, 1100-1109, doi:10.1161/01.res.79.6.1100 (1996).
12 Meissner, G. & Henderson, J. S. Rapid calcium release from cardiac sarcoplasmic reticulum vesicles is dependent on Ca2+ and is modulated by Mg2+, adenine nucleotide, and calmodulin. *J Biol Chem* **262**, 3065-3073 (1987).
13 Balshaw, D., Gao, L. & Meissner, G. Luminal loop of the ryanodine receptor: a pore-forming segment? *Proc Natl Acad Sci U S A* **96**, 3345-3347, doi:10.1073/pnas.96.7.3345 (1999).
14 Quinn, K. E., Castellani, L., Ondrias, K. & Ehrlich, B. E. Characterization of the ryanodine receptor/channel of invertebrate muscle. *Am J Physiol* **274**, R494-502, doi:10.1152/ajpregu.1998.274.2.R494 (1998).
15 Ahern, G. P., Junankar, P. R. & Dulhunty, A. F. Subconductance states in single-channel activity of skeletal muscle ryanodine receptors after removal of FKBP12. *Biophys J* **72**, 146-162, doi:10.1016/S0006-3495(97)78654-5 (1997).
16 Chen, S. R. *et al.* Single-channel properties of the recombinant skeletal muscle Ca2+ release channel (ryanodine receptor). *Biophys J* **73**, 1904-1912, doi:10.1016/S0006-3495(97)78221-3 (1997).
17 Smith, J. S. *et al.* Purified Ryanodine Receptor from Rabbit Skeletal-Muscle Is the Calcium-Release Channel of Sarcoplasmic-Reticulum. *J Gen Physiol* **92**, 1-26, doi:DOI 10.1085/jgp.92.1.1 (1988).
18 Mitchell, R. D., Simmerman, H. K. & Jones, L. R. Ca2+ binding effects on protein conformation and protein interactions of canine cardiac calsequestrin. *J Biol Chem* **263**, 1376-1381 (1988).
19 Jones, L. R., Zhang, L., Sanborn, K., Jorgensen, A. O. & Kelley, J. Purification, primary structure, and immunological characterization of the 26-kDa calsequestrin binding protein (junctin) from cardiac junctional sarcoplasmic reticulum. *Journal of Biological Chemistry* **270**, 30787-30796, doi:DOI 10.1074/jbc.270.51.30787 (1995).
20 Wei, L., Gallant, E. M., Dulhunty, A. F. & Beard, N. A. Junctin and triadin each activate skeletal ryanodine receptors but junctin alone mediates functional interactions with calsequestrin. *Int J Biochem Cell B* **41**, 2214-2224, doi:10.1016/j.biocel.2009.04.017 (2009).
21 Guo, W. & Campbell, K. P. Association of triadin with the ryanodine receptor and calsequestrin in the lumen of the sarcoplasmic reticulum. *J Biol Chem* **270**, 9027-9030, doi:10.1074/jbc.270.16.9027 (1995).
22 Li, L. W. *et al.* A new cytoplasmic interaction between junctin and ryanodine receptor Ca2+ release channels. *J Cell Sci* **128**, 951-963, doi:10.1242/jcs.160689 (2015).
23 Yan, Z. *et al.* Structure of the rabbit ryanodine receptor RyR1 at near-atomic resolution. *Nature* **517**, 50-+, doi:10.1038/nature14063 (2015).
24 Zalk, R. *et al.* Structure of a mammalian ryanodine receptor. *Nature* **517**, 44-49, doi:10.1038/nature13950 (2015).
25 des Georges, A. *et al.* Structural Basis for Gating and Activation of RyR1. *Cell* **167**, 145-157 e117, doi:10.1016/j.cell.2016.08.075 (2016).
26 Gong, D. *et al.* Modulation of cardiac ryanodine receptor 2 by calmodulin. *Nature* **572**, 347-351, doi:10.1038/s41586-019-1377-y (2019).
27 Iyer, K. A. *et al.* Structural mechanism of two gain-of-function cardiac and skeletal RyR mutations at an equivalent site by cryo-EM. *Sci Adv* **6**, doi:ARTN eabb2964.10.1126/sciadv.abb2964 (2020).
28 Ma, R. *et al.* Structural basis for diamide modulation of ryanodine receptor. *Nat Chem Biol* **16**, 1246-1254, doi:10.1038/s41589-020-0627-5 (2020).
29 Sanchez, R. M., Zhang, Y., Chen, W., Dietrich, L. & Kudryashev, M. Subnanometer-resolution structure determination in situ by hybrid subtomogram averaging - single particle cryo-EM. *Nat Commun* **11**, 3709, doi:10.1038/s41467-020-17466-0 (2020).
30 Woll, K. A., Haji-Ghassemi, O. & Van Petegem, F. Pathological conformations of disease mutant Ryanodine Receptors revealed by cryo-EM. *Nat Commun* **12**, 807, doi:10.1038/s41467-021-21141-3 (2021).
31 Melville, Z., Kim, K., Clarke, O. B. & Marks, A. R. High-resolution structure of the membrane-embedded skeletal muscle ryanodine receptor. *Structure* **30**, 172-180 e173, doi:10.1016/j.str.2021.08.001 (2022).
32 Wei, R. *et al.* Structural insights into Ca(2+)-activated long-range allosteric channel gating of RyR1. *Cell Res* **26**, 977-994, doi:10.1038/cr.2016.99 (2016).
33 Efremov, R. G., Leitner, A., Aebersold, R. & Raunser, S. Architecture and conformational switch mechanism of the ryanodine receptor. *Nature* **517**, 39-43, doi:10.1038/nature13916 (2015).
34 Bai, X. C., Yan, Z., Wu, J. P., Li, Z. Q. & Yan, N. The Central domain of RyR1 is the transducer for long-

range allosteric gating of channel opening. *Cell Research* **26**, 995-1006, doi:10.1038/cr.2016.89 (2016).
35 Willegems, K. & Efremov, R. G. Influence of Lipid Mimetics on Gating of Ryanodine Receptor. *Structure* **26**, 1303-1313 e1304, doi:10.1016/j.str.2018.06.010 (2018).
36 Chi, X. *et al.* Molecular basis for allosteric regulation of the type 2 ryanodine receptor channel gating by key modulators. *Proc Natl Acad Sci U S A* **116**, 25575-25582, doi:10.1073/pnas.1914451116 (2019).
37 Lai, F. A., Erickson, H. P., Rousseau, E., Liu, Q. Y. & Meissner, G. Purification and reconstitution of the calcium release channel from skeletal muscle. *Nature* **331**, 315-319, doi:10.1038/331315a0 (1988).
38 Yin, C. C. & Lai, F. A. Intrinsic lattice formation by the ryanodine receptor calcium-release channel. *Nat Cell Biol* **2**, 669-671, doi:10.1038/35023625 (2000).
39 Wang, S. R. *et al.* Crystal structure of calsequestrin from rabbit skeletal muscle sarcoplasmic reticulum. *Nat Struct Biol* **5**, 476-483, doi:DOI 10.1038/nsb0698-476 (1998).
40 Samso, M. A guide to the 3D structure of the ryanodine receptor type 1 by cryoEM. *Protein Sci* **26**, 52-68, doi:10.1002/pro.3052 (2017).
41 Zheng, S. Q. *et al.* MotionCor2: anisotropic correction of beam-induced motion for improved cryo-electron microscopy. *Nat Methods* **14**, 331-332, doi:10.1038/nmeth.4193 (2017).
42 Zhang, K. Gctf: Real-time CTF determination and correction. *J Struct Biol* **193**, 1-12, doi:10.1016/j.jsb.2015.11.003 (2016).
43 Zivanov, J. *et al.* New tools for automated high-resolution cryo-EM structure determination in RELION-3. *Elife* **7**, doi:10.7554/eLife.42166 (2018).
44 Punjani, A., Zhang, H. & Fleet, D. J. Non-uniform refinement: adaptive regularization improves single-particle cryo-EM reconstruction. *Nat Methods* **17**, 1214-1221, doi:10.1038/s41592-020-00990-8 (2020).
45 Heymann, J. B. & Belnap, D. M. Bsoft: image processing and molecular modeling for electron microscopy. *J Struct Biol* **157**, 3-18, doi:10.1016/j.jsb.2006.06.006 (2007).
46 Pettersen, E. F. *et al.* UCSF Chimera--a visualization system for exploratory research and analysis. *J Comput Chem* **25**, 1605-1612, doi:10.1002/jcc.20084 (2004).
47 Adams, P. D. *et al.* The Phenix software for automated determination of macromolecular structures. *Methods* **55**, 94-106, doi:10.1016/j.ymeth.2011.07.005 (2011).
48 Emsley, P., Lohkamp, B., Scott, W. G. & Cowtan, K. Features and development of Coot. *Acta Crystallogr D Biol Crystallogr* **66**, 486-501, doi:10.1107/S0907444910007493 (2010).
49 Smart, O. S., Neduvelil, J. G., Wang, X., Wallace, B. A. & Sansom, M. S. HOLE: a program for the analysis of the pore dimensions of ion channel structural models. *J Mol Graph* **14**, 354-360, 376, doi:10.1016/s0263-7855(97)00009-x (1996).

Figures

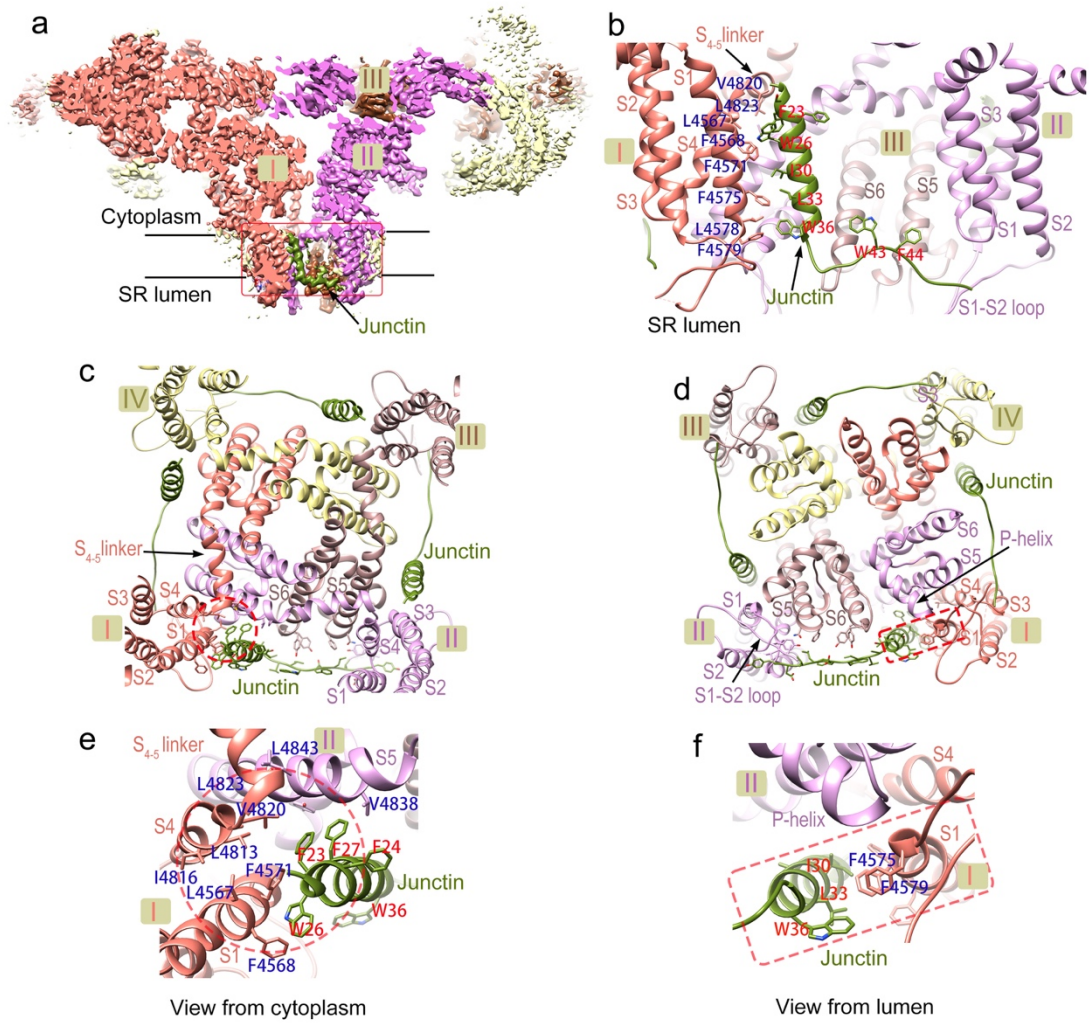

Fig.1 The structure of RyR-junctin complex and binding sites of junctin. (a) the cryo-EM density of RyR1-junctin complex shows an extra density indicating the junctin TM helix with a small loop in lumen (dark green). Two RyR sub-units (pink and purple) are shown in cutting section to allow a clear visualization of junctin. The model of RyR-junctin in TM and luminal domain (red box in a) are illustrated in side-view(b), top-bottom view(c) and bottom-top view(d). (e) and (f) are enlarged regions from (c, circle) and (d, rectangle), respectively. I, II, III and IV represent four sub-units in RyR1 tetramer.

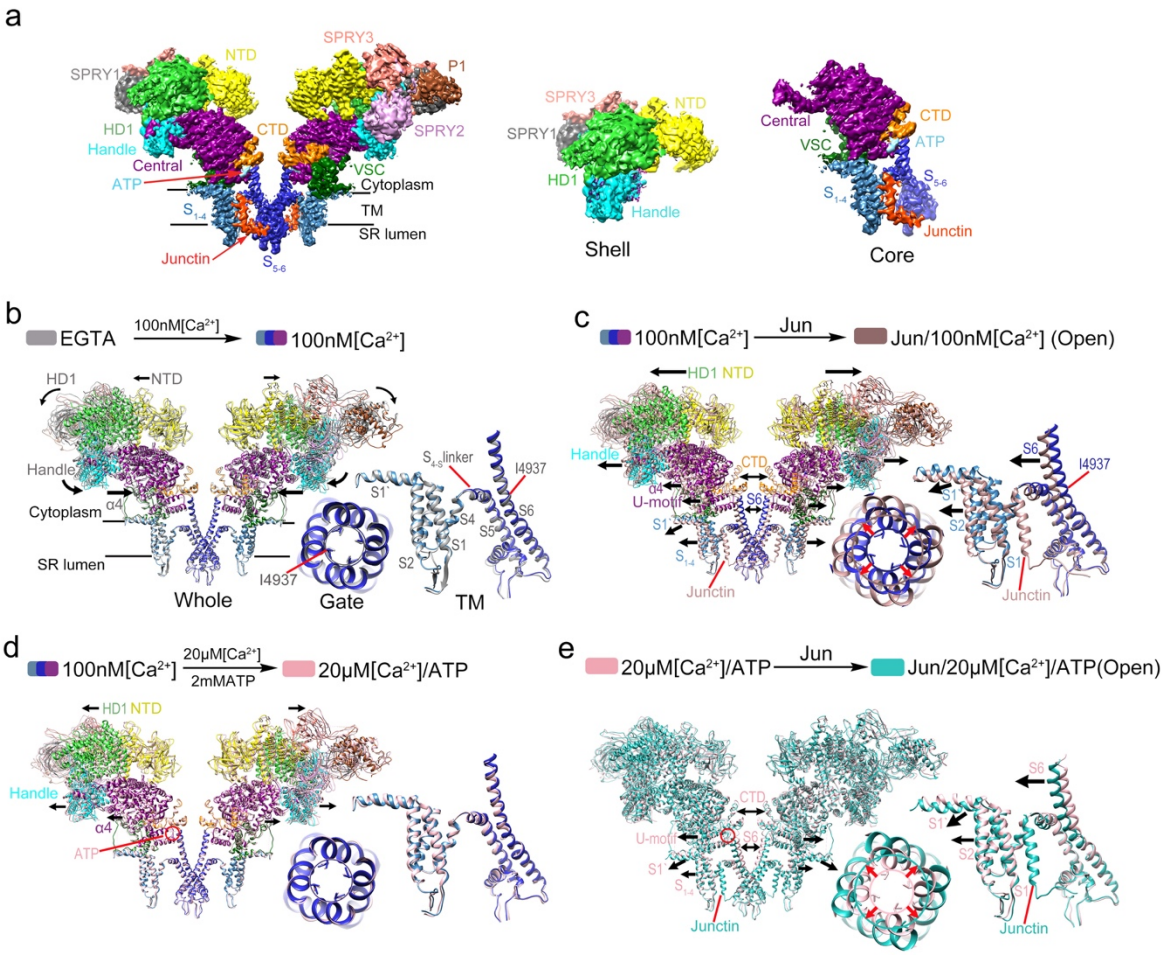

Fig.2 Conformational transitions of the whole and TM domain in RyR1 in different structures. (a) Structural illustration of domain organization. (b) Conformational transitions of purified RyR1 after Ca^{2+} loading. Condition 1(RyR1-EGTA) is shown in grey; condition 2 (RyR1-100nM [Ca^{2+}]) is colored by domains. HD1, green; NTD, yellow; Handle, cyan; central domain, purple; CTD, brown; S_{1-4}, light blue; S_{5-6}, blue. (c) Conformational transitions from purified RyR1(condition 2, same color scheme as panel b) to native RyR1-junctin in nM Ca^{2+} (condition 3, brownish red). (d) Conformational transitions of purified RyR1 from condition 2 (same color scheme as (b)) to condition 4 (pink). (e) Conformational transitions of RyR1-junctin from condition 4 (RyR1-μM[Ca^{2+}]/ATP, pink) to condition 5 (RyR1-Jun/μM[Ca^{2+}]/ATP, teal). The insets show enlarged transmembrane structures and conformational change of the gate (I4937). Jun=junctin.

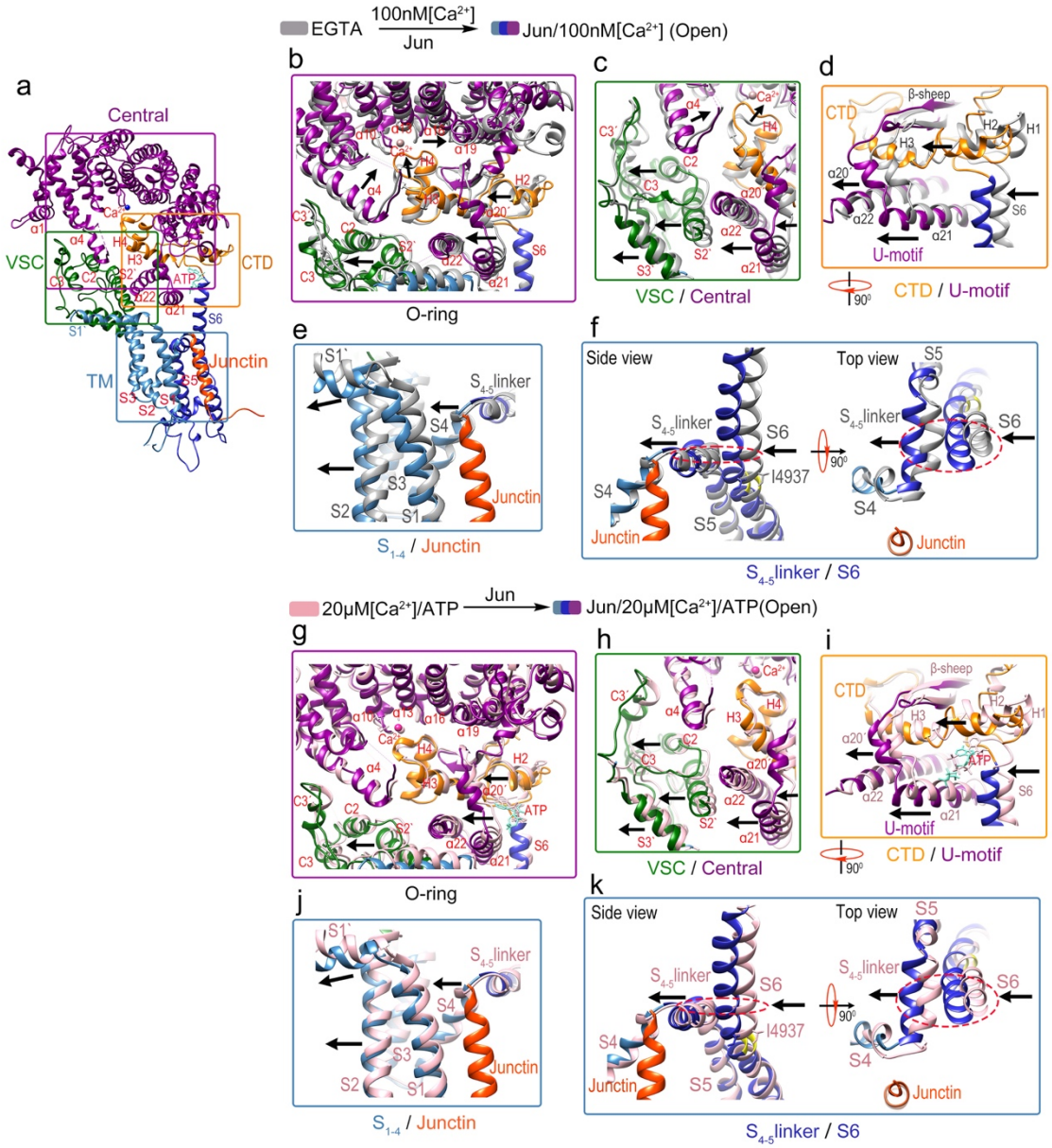

549

550 Fig.3 Conformational transitions of the core region (central domain, VSC, CTD, S_{1-4} and S_{4-5}
551 linker) in RyR1 functional state. (a) Structural illustration of domain organization: central
552 domain, purple; VSD, green; CTD, brown; S_{1-4}, light blue; S_{5-6}, blue. (b)-(f) show the domain
553 transitions from closed state (condition 1, grey) to activated open state (condition 3, colored).
554 (g)-(k) show the domain transitions from pre-open state (condition 4, pink) to full open state
555 (condition 5, colored). Jun=junctin.

556

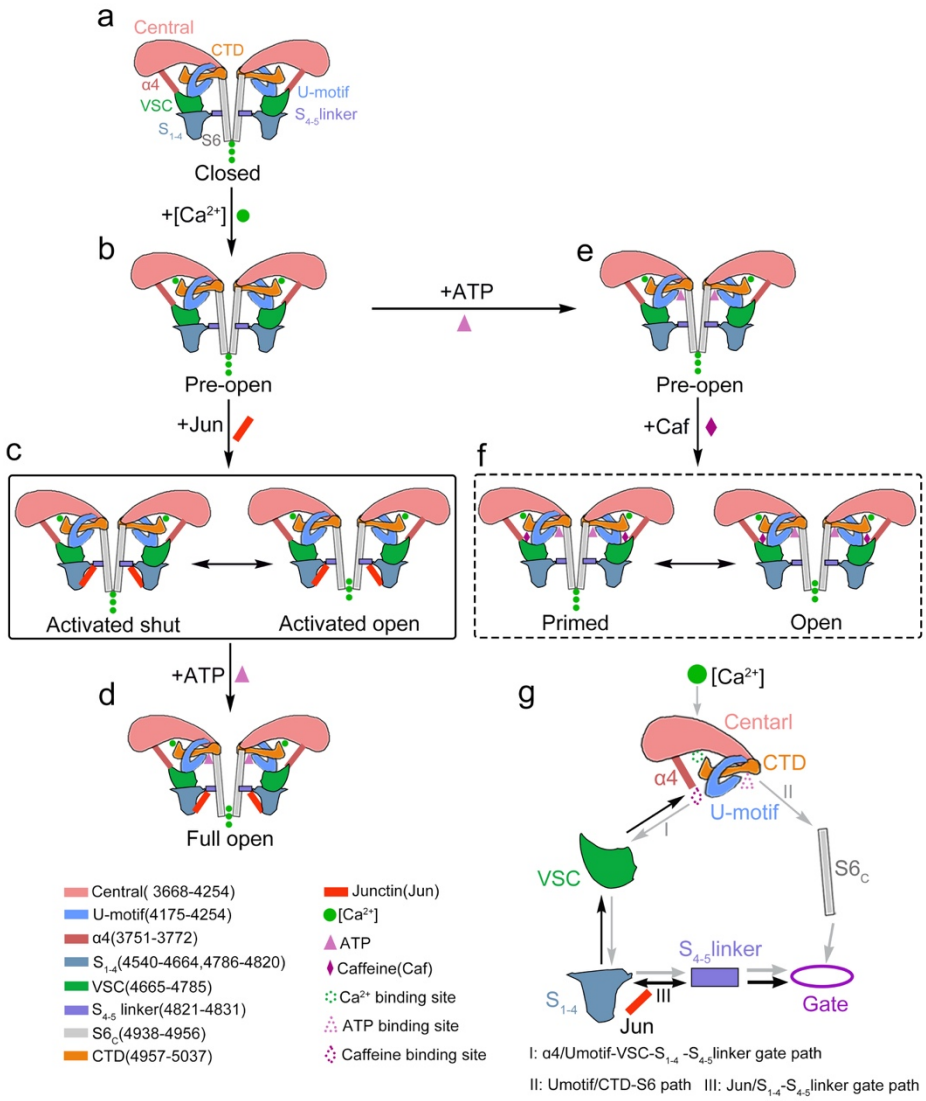

Fig.4 The modulation of RyR1 by Ca^{2+}, ATP, Caffeine and junctin. Two opposite monomers are displayed with domains in cartoon. (a) RyR1 in rest state without Ca^{2+} and the channel is closed. (b) In the presence of Ca^{2+}, RyR1 is in pre-open state with a closed gate. (c) In the presence of Ca^{2+} and junctin, RyR1s have two conformations (solid box), which are activated shut (gate is closed) and activated open states (gate is open). (d) In the presence of Ca^{2+}, ATP and junctin, RyR1 is in full open state. (e) In the presence of Ca^{2+} and ATP, RyR1 is in pre-open state with a closed gate. (f) In the presence of Ca^{2+}, ATP and exogenous regulator (e.g. Caffeine), RyR1 have two conformations (dashed box), which are primed (gate is closed) and open states (37% of particles, gate is open)[31]. (g) Schematic diagram of RyR gating mechanism. Ca^{2+}/ATP/Caf regulate the channel through α4/Umotif-VSC-S_{1-4}–S_{4-5} linker-gate path and Umotif/CTD-S6 path, as indicated by the gray arrows. Junctin regulates the channel through Jun/S_{1-4}–S_{4-5} linker-gate path, as indicated by the black arrows.

Extended data figure/table legends

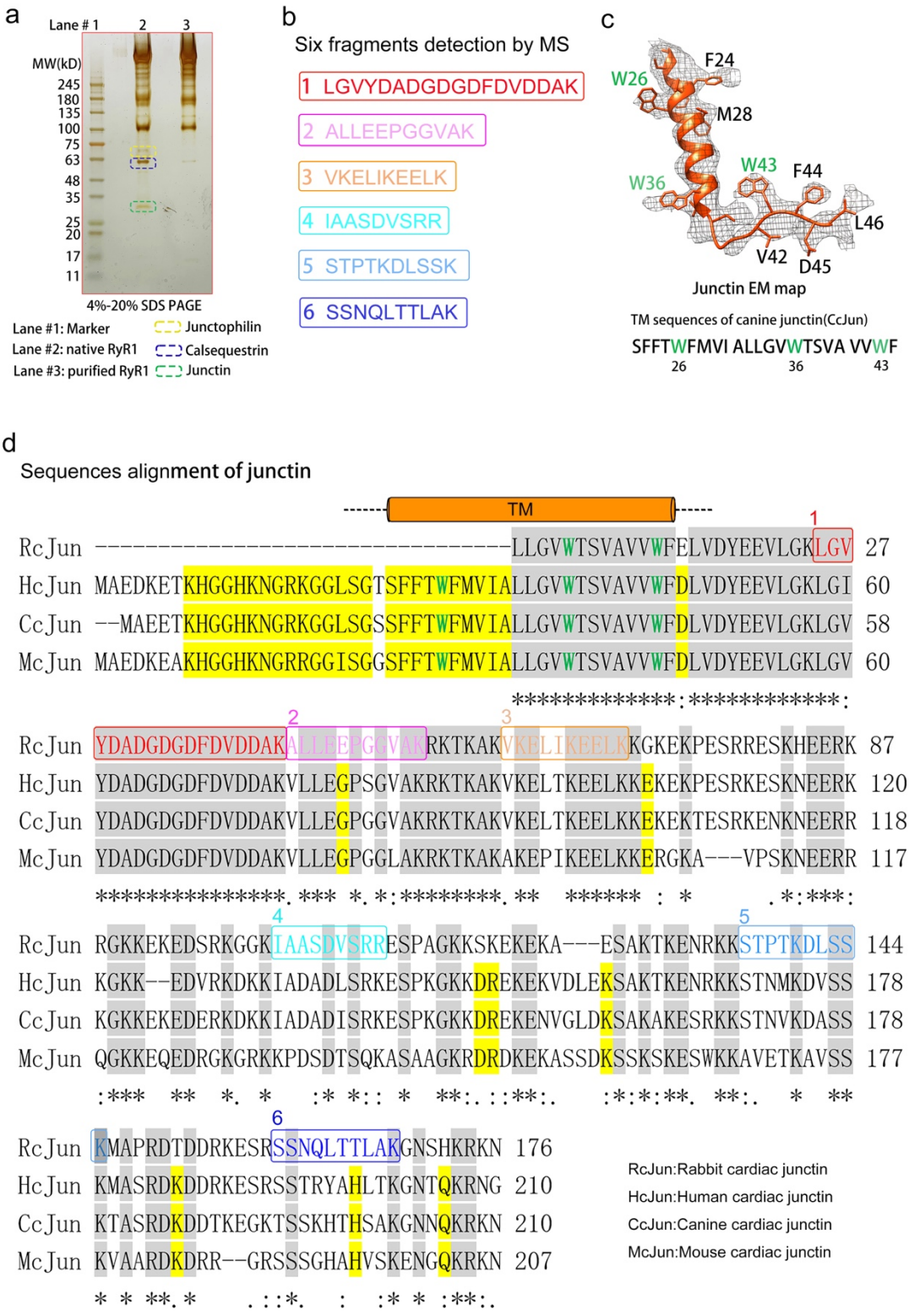

Fig.S1 Identification of junctin from the mild purified RyR1. (a) The SDS-PAGE of mild purified RyR1(denoted as native RyR1) (lane#2) and regularly purified RyR1(denoted as purified RyR1) (lane#3). Boxes show the position of junctophilin, calsequestrin and junctin,

575 respectively. (b) Mass spectroscopy analysis located six finger print fragments (six boxes). (c)
576 The model of junctin fits into the extra density in the mild purified RyR1 structure. (d)
577 Sequence alignment of junctin from rabbit, human, canine and mouse, indicating junctin has
578 high homology.
579

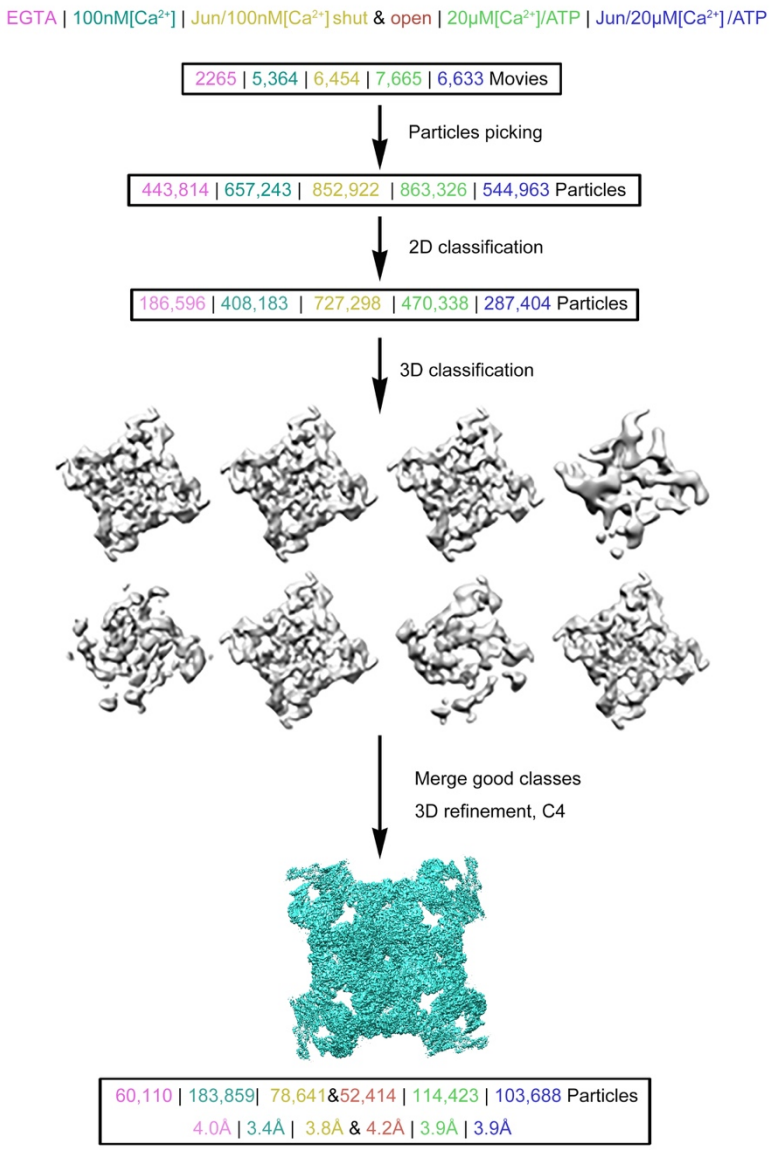

Fig.S2 Flow chart of cryo-EM data processing. Five RyR1 samples under conditions 1-5 are imaged and processed: condition 1, RyR1-EGTA in closed state, pink; condition 2, RyR1-100nM[Ca^{2+}] in pre-open state, cyan; condition 3, RyR1-Jun/nM[Ca^{2+}], two structures in shut and open state are obtained (yellow and salmon); condition 4, RyR1-μM[Ca^{2+}]/ATP in pre-open state, green; condition 5, RyR1-Jun/μM[Ca^{2+}]/ATP in full open state, blue.

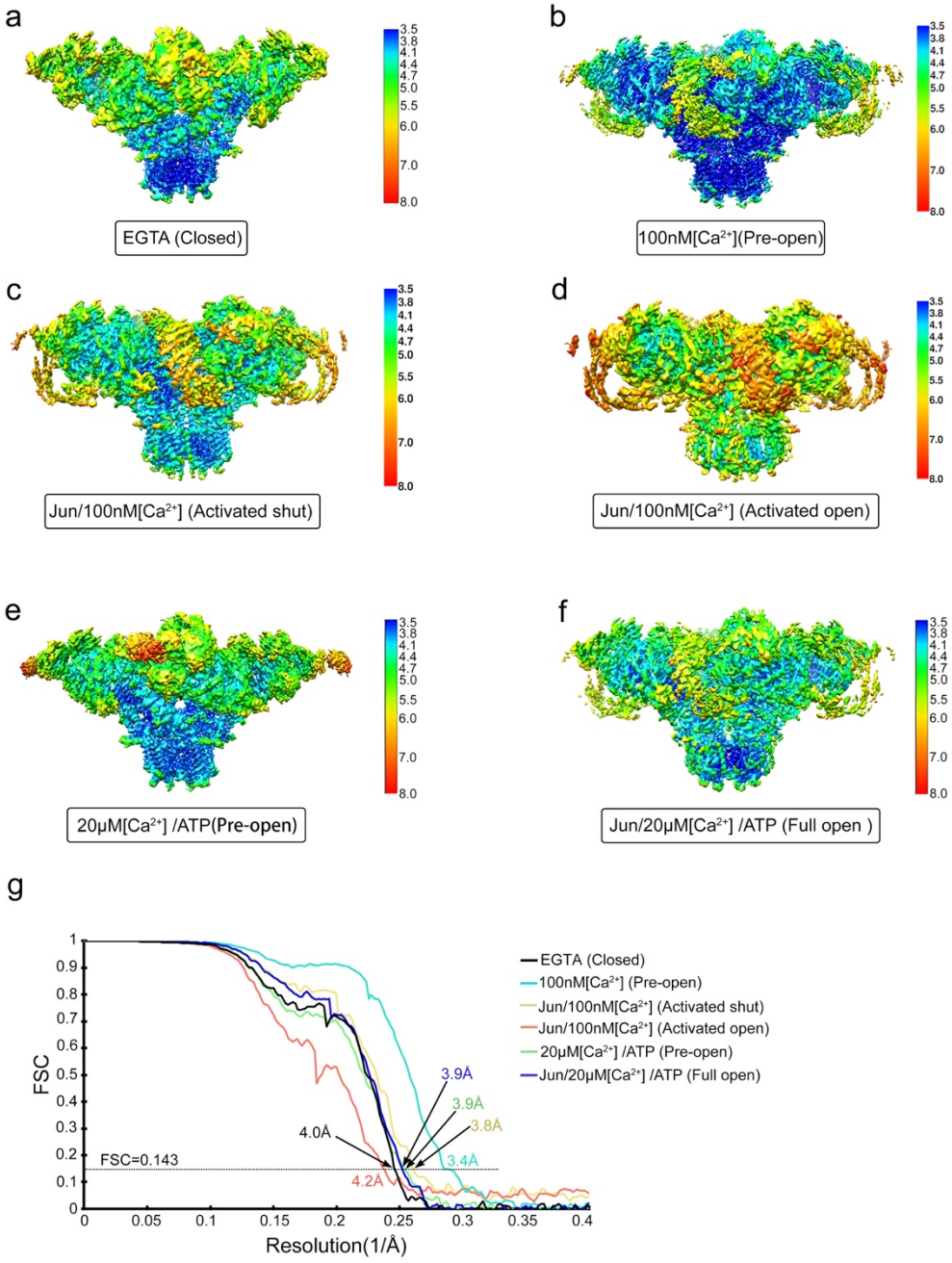

587

588 Fig.S3 Local resolution maps and FSC curves of the six reconstructions calculated by blocres

589 and cryoSPARC.

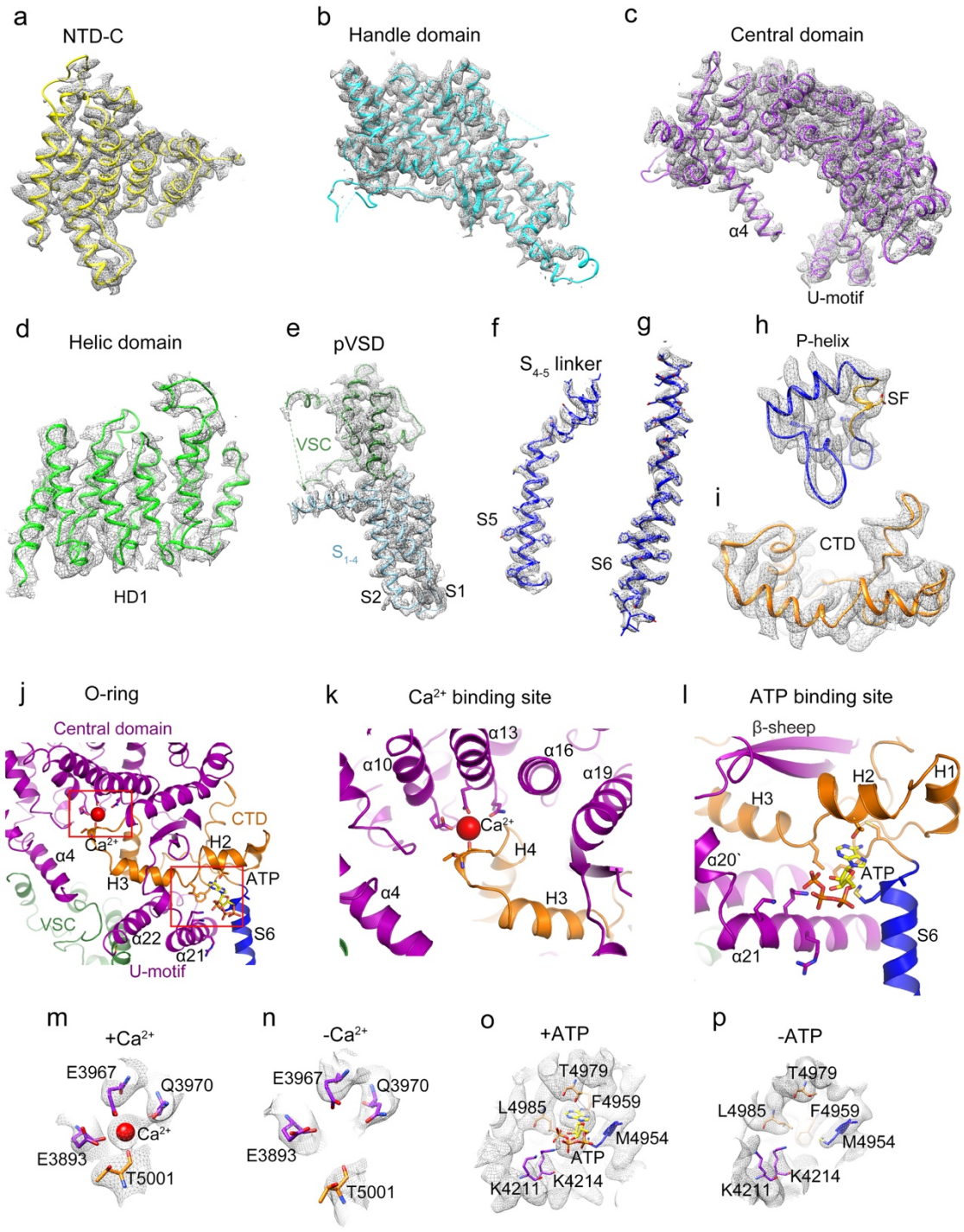

Fig.S4 Representative densities from the electron microscopy maps. (a)-(i) The models fit with density maps of NTD-C, Handle domain, Central domain, Helical domain (HD1), pVSD (VSC and S_{1-4}), S5, S6, selective filter (SF) and P-helix, and CTD, respectively. (j) The model of O-ring. (k, m, n) show the structures of Ca^{2+} binding sites with and without Ca^{2+}. (l, o, p) The structures of ATP binding sites with and without ATP.

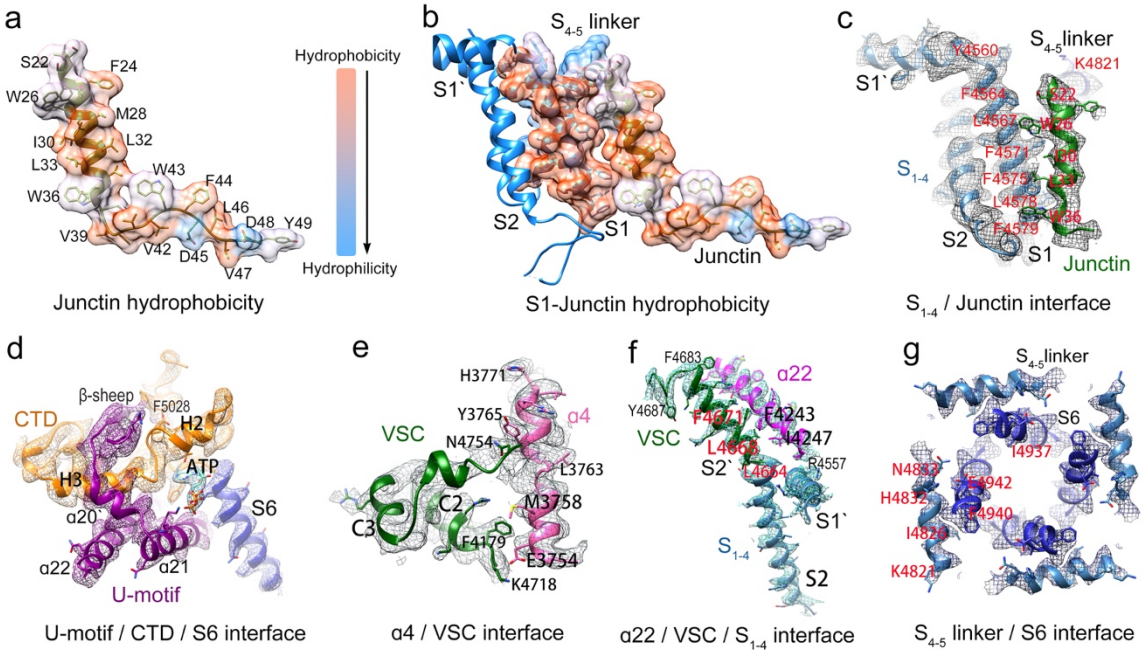

597 Fig.S5 Representative domains that participate in the conformational transitions. (a) and (b)
598 are hydrophobic surface of junctin and S1, S_{4-5} linker of RyR1. (c)-(g) cryoEM densities of
599 interface between junctin and RyR1, and interfaces among the key domains in core region.

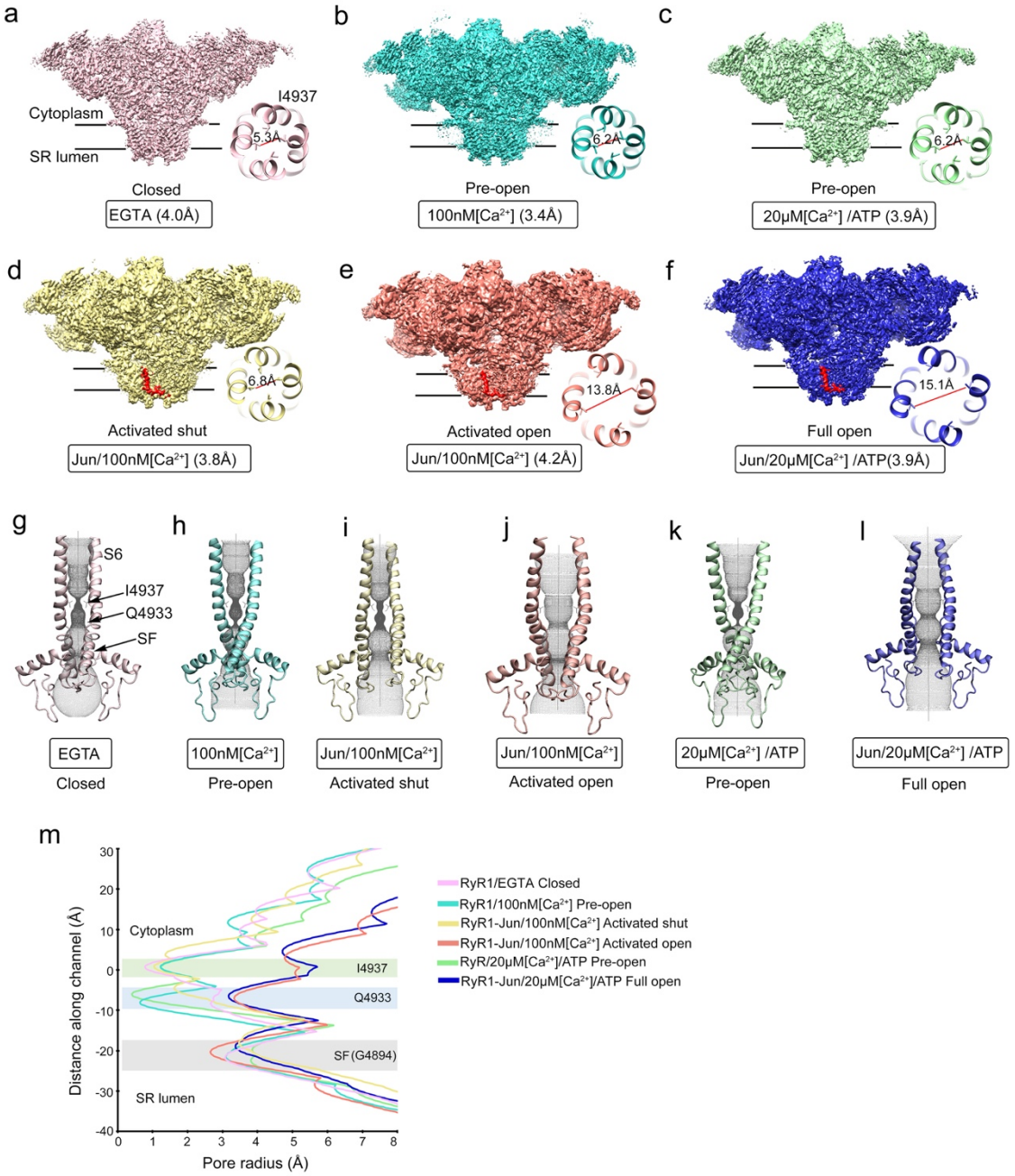

600

601 Fig.S6 The side-view of the six reconstructions and pore conformations. Insets of (a)-(f)
602 show the gate diameters by measuring two opposing residues I4937. (g)-(m) are the pore
603 calculation of the ion permeation path, measured by HOLE. SF=selective filter.

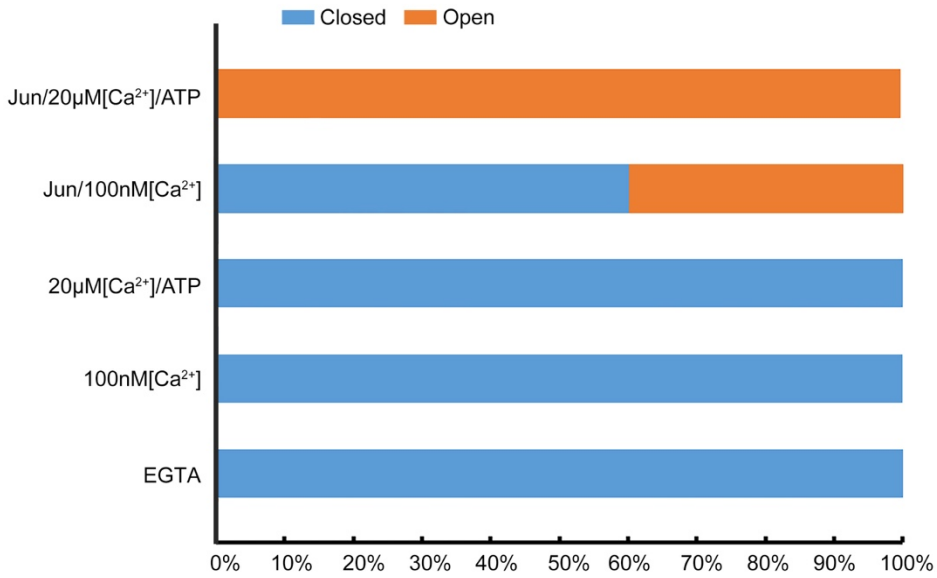

Fig.S7 Proportions of closed and open particles in the RyR1 samples at conditions 1, 2, 3, 4 and 5. In condition 1 (EGTA), 2 (100nM [Ca^{2+}]) and 4 (20μM[Ca^{2+}]/ATP), the gate is closed. In condition 3 (Jun/100nM [Ca^{2+}]), both closed gate and open gate are observed, with 60% and 40% particles, respectively. In condition 5 (Jun/20μM[Ca^{2+}]/ATP), the gate is open.

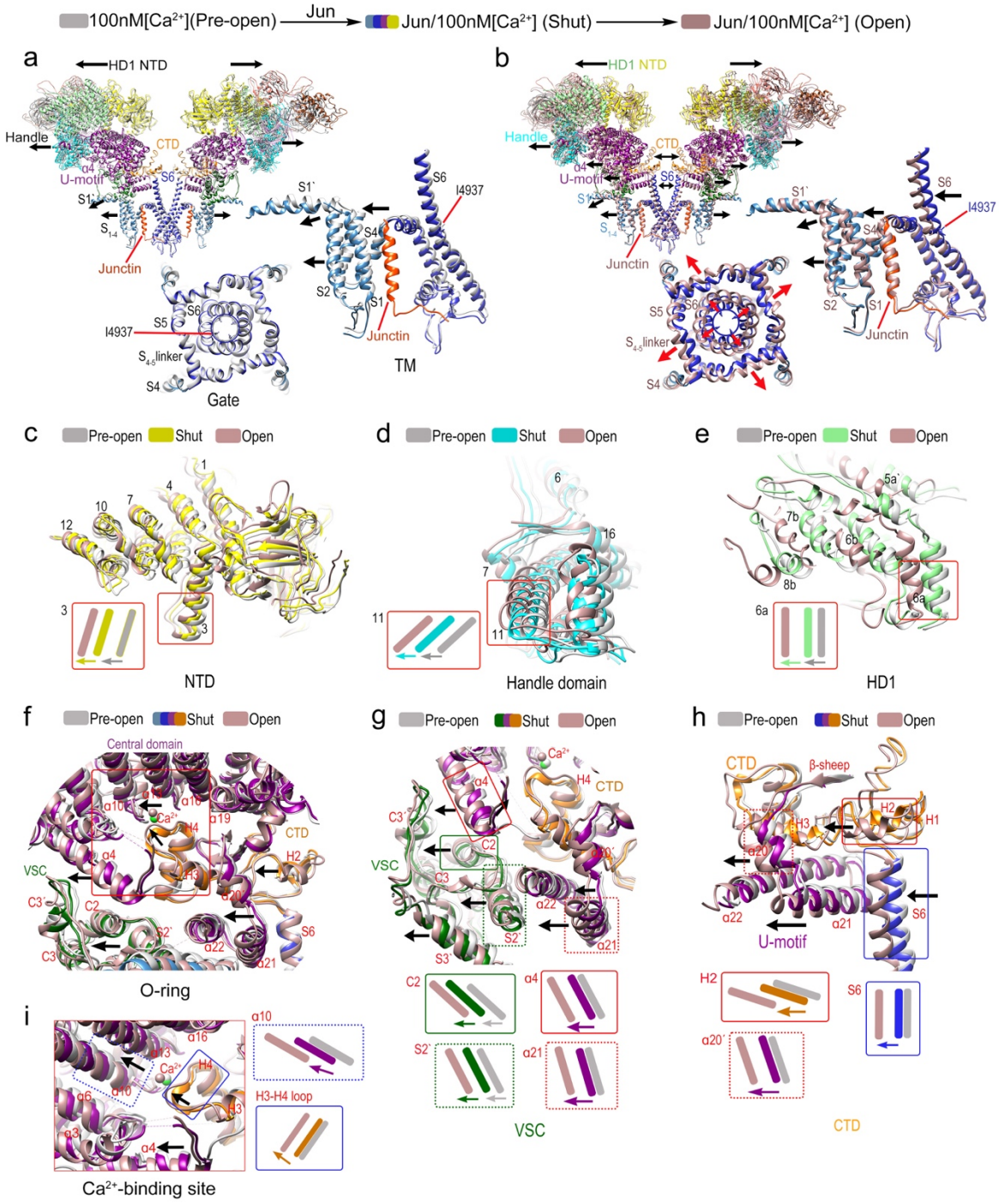

609

610 Fig.S8 The conformation transitions among pre-open, shut and open states. (a) The comparison
611 between shut (colored by domains) and pre-open(grey) states. In shut state, the shell
612 region(NTD、HD1 and handle domain) moves outward and TM $S_{1\text{-}4}$ also moves outward. α4,
613 U-motif and CTD remain the same conformation as pre-open state. The insets highlight the
614 TM region and the gate. The helix S1', S1, and S2 have an outward shift but S6 remains still
615 so the gate is closed. (b) The comparison between shut (colored by domains) and open(brown)

states. In open state, the shell region and core region (α4, U-motif and CTD) move outward from the central axis. The insets highlight the structures of TM region and the gate. The helix S1', S1, S2 and S6 have an outward shift so the gate is open. (c)-(i) the movement of the key domains during conformational transitions. The insets show the movement of helix in NTD, Handle domain, HD1, α4, U-motif, VSC, CTD and S6 in cartoon.

622

623 Table. S1 Summary of data collection and model statistics.

Dataset	EGTA (closed)	nM[Ca^{2+}] (Pre-open)	Jun/nM[Ca^{2+}] (Activated shut)	Jun/nM[Ca^{2+}] (Activated open)	μM[Ca^{2+}]/ATP (Pre-open)	Jun/μM[Ca^{2+}]/ATP (Full open)
EMDB						
PDB						
Ligand						
$[Ca^{2+}]_{free}$	-	100nM	100nM	100nM	20μM	20μM
ATP	-	-	-	-	2mM	2mM
EGTA	5mM	-	-	-	-	-
Data collection						
Electron Microscope	FEI Titan Krios					
Voltage (kV)	300					
Detector	Falcon-III/K3					
Pixel size (Å)	1.09/0.855					
Electron dose ($e^-/Å^2$)	50					
Defocus rang(μm)	-1.2 to -2.2					
Reconstruction						
Software	RELION 3.0/3.1/CryoSPARC					
Symmetry	C4					
Number of Particles	60,110	183,859	78,641	52,414	114,423	103,688
Final resolution (Å)	4.0	3.4	3.8	4.2	3.9	3.9
Map sharpening B-factor ($Å^2$)	-164.4	-160.4	-126	-136.5	-194.5	-143.8
Model building						
Software	COOT					
Refinement						
Software	PHENIX					
Validation						

R.m.s deviations						
Bonds length(Å)	0.003	0.004	0.004	0.004	0.004	0.002
Bonds angle(Å)	0.618	0.601	0.987	0.991	0.928	0.494
Ramachandran plot statistics (%)						
Preferred	90.80	91.05	91.75	90.74	90.64	91.53
Allowed	9.12	8.84	8.25	9.2	9.34	8.47
Outlier	0.08	0.11	0	0.07	0.03	0
Rotamer outliers (%)	0	0.45	0	0.22	0.00	0.04
MolProbity score	2.01	2.09	1.97	2.20	2.67	1.87

624

625

626

627 Table. S2 RyR1 Domain Definitions

628

Domain symbol definition in Zalk, R et al [24]	**Domain symbol in this paper (Yan Z et al [23])**
Shell:1-3613	
NTD-A: N-terminal domain A (1-208) NTD-B: N-terminal domain B (209-392) Nsol: N-terminal solenoid (393–627)	NTD: N-terminal domain (1-631) NTD-A (1-205), NTD-B (206-394), NTD-C (395-631)
SPRY1: SP1a/ryanodine receptor domain 1 (628–849) SPRY2: SP1a/ryanodine receptor domain 2 (1055–1241) SPRY3: SP1a/ryanodine receptor domain 3 (1242–1656)	SPRY1 (632-826,1466-1491,1615-1634) SPRY2 (827-857,1070-1241) SPRY3 (1242-1614)
RY1&2: RYR repeats 1 and 2 (850–1054) RY3&4: RYR repeats 3 and 4 (2735–2938)	P1 (858-1055) P2 (2734-2940)
JSol: junctional solenoid (1657–2144)	Handle domain (1651-2145)
BSol: bridging solenoid (2145–3613)	Helical domain: HD1 (2146-2712); HD2 (3016-3572)
Channel and Core: 3614–5037	
SCLP: shell-core linker peptide (3614–3666) CSol: core solenoid (3667–4174) TaF: thumb and Forefingers domain (4175–4253)	Central domain (3668-4254) α_4 (3751-3772) U-motif: U-shaped subdomain (4175-4254)
pVSD: pseudo voltage sensor domain from S1´to S4 (4541–4819) S2S3: helical-bundle domain between S2 and S3 (4666–4786)	$S_{1\text{-}4}$: S1´, S1, S2, S3, S4, (4540-4664, 4786-4820) VSC: voltage-sensor like domain between S2 and S3 (4665-4785)
Pore: channel pore domain (4820–4956) S6c: cytoplasmic extension of S6 (4938–4956) Gate: Ile4937	$S_{4\text{-}5}$ linker: S4-S5 linker (4821-4831) $S_{5\text{-}6}$: channel helices S5-S6(4832–4956) S6c: cytoplasmic extension (4938–4956) of S6 Gate: Ile4937
CTD: C-terminal domain (4957–5037)	CTD: C-terminal domain (4957–5037)

629

Supplementary Files

This is a list of supplementary files associated with this preprint. Click to download.

- TableS1Summaryofdatacollectionandmodelstatistics.pdf
- TableS2RyR1DomainDefinitions20220308.pdf
- FigS1.jpg
- FigS2.jpg
- FigS3.jpg
- FigS4.jpg
- FigS5.jpg
- FigS6.jpg
- FigS7.jpg
- FigS8.jpg